Uncommon Optical Properties and Silver-responsive Turn-off/on Luminescence in a Pt(II) heteroleptic dithiolene complex

Salahuddin S. Attar,[a] Flavia Artizzu,[b] Luciano Marchiò,*[c] Davide Espa,[a] Luca Pilia,[d] Maria F. Casula,[a] Angela Serpe,[e] Maddalena Pizzotti,[f] Alessio Orbelli Biroli[g] and Paola Deplano*[a]

Abstract: The complex [Pt(*i*-Pr$_2$pipdt)(Quinoxdt)] (*i*-Pr$_2$pipdt = 1,4-di-isopropyl-piperazine-2,3-dithione; Quinoxdt= [1,4]dithiino[2,3-b]quinoxaline-2,3-dithiolate) exhibits a remarkable green emission at 570 nm (room temperature), which is above the lowest excited state. The complex is characterized by negative solvatochromism as well as a high second-order polarizability. Addition of Ag(I) ions induces i) hypsochromic shift of the lowest frequencies; and ii) reversible quenching of luminescence. The corresponding Ni and Pd complexes have been also prepared and investigated to assist interpretation of optical properties within the triad. Computational studies based on density functional theory and time-dependent theory highlight the electronic properties of [Pt(i-Pr$_2$pipdt)(Quinoxdt)]. The preferential site of interaction between the Pt complex and incoming Ag(I) is evidenced by shape of the Fukui functions, pointing to the thiolic sulfur and platinum atoms as the most reactive sites towards a soft cation. Calculated optical properties are in agreement with experimental findings. This study contributes to shed light on the structure-properties relationship for this class of compounds

[a] Dr S. S. Attar, Dr D. Espa, Prof M. F. Casula, Prof P. Deplano
Department of Chemical and Soil Sciences
University of Cagliari, INSTM Research Unit
09042 Monserrato (CA), Italy
E mail: deplano@unica.it
[b] Dr F. Artizzu
L^3 – Luminescent Lanthanide Lab, Department of Chemistry
Ghent University
Krijgslaan 281 – building S3, B-9000 Gent, Belgium
[c] Prof L. Marchiò
Dipartimento di Scienze Chimiche, della Vita e della Sostenibilità Ambientale
Università di Parma
Parco Area delle Scienze 11/a, 43124 Parma, Italy
E-mail: luciano.marchio@unipr.it
[d] Dr L. Pilia
Dipartimento di Ingegneria Meccanica, Chimica e dei Materiali
Università di Cagliari
Via Marengo 2, 09123 Cagliari, Italy
[e] Dr A. Serpe
Dipartimento di Ingegneria Civile, Ambientale e Architettura
Università di Cagliari
Via Marengo 2, 09123 Cagliari, Italy
[f] Prof M. Pizzotti
Department of Chemistry, INSTM Research Unit,
University of Milan
Via C. Golgi 19, 20133 Milano, Italy
[g] Dr A. Orbelli Biroli
Istituto di Scienze e Tecnologie Molecolari del CNR (CNR-ISTM),
SmartMatLab Centre,
CNR
Via C. Golgi 19, 20133 Milano, Italy 1

Supporting information for this article is given via a link at the end of the document.((Please delete this text if not appropriate))

Introduction

Homoleptic and heteroleptic metal dithiolene complexes feature peculiar electronic structures, which result in relevant properties for several applicative fields proper of molecular materials.[1a-c] Square-planar heteroleptic d^8 metal-dithiolene complexes have been shown to be suitable candidates to work as tunable second-order nonlinear optical (NLO) chromophores.[2] The requirement to obtain this property is the presence of two ligands occurring in formally different oxidation states, one reducing (dianionic dithiolate, electron donor), and the other oxidizing (neutral dithione, electron acceptor). These non-centrosymmetric molecules exhibit an absorption peak in the visible spectral region, which is tunable with the HOMO–LUMO energy gap. Specifically, the donor gives a prevailing contribution to the HOMO, and the acceptor mainly contributes to the LUMO, with the coordinated metal acting as a π-bridge for the electron transfer. Accordingly, the Charge Transfer (CT) donor-acceptor process produces a decrease of the dipole moment from the ground to the excited state and, as a consequence, negative solvatochromism and first hyperpolarizability (β) is observed.[3]

Interestingly, the extensively investigated dithione-dithiolato complexes, including [Pt(*i*-Pr$_2$pipdt)(dmit)] (dmit= 2-thioxo-1,3-dithiole-4,5-dithiolato), do not exhibit luminescence in solution at room temperature or in glassy solvents at 77 K.[4] On the other hand, heteroleptic platinum diimine-dithiolato (diimine: acceptor, dithiolate: donor) exhibit both 2nd NLO activity and luminescence associated with the CT transition.[5] Recently, we have reported both homoleptic and heteroleptic platinum complexes with the Quinoxdt ligand (donor) that are emissive in solution and at room temperature (RT). Remarkably, it was observed that the emission falls above the energy of the lowest-energy absorption, pointing to an apparent “anti-Kasha” behavior (Figure S1).[6] In the homoleptic case, [Pt(Quinoxdt)$_2$]$^-$ (see Figure 1), irradiation at 420 nm yields an emission peak at 572 nm, well above in energy to the lowest absorption peak at 1085 nm, which is associated to the HOMO−1→SOMO transition.[7] In the heteroleptic case, the [Pt(MBA)(Quinoxdt)]$^-$ complex (MBA: (R)-α-MBAdto dithioxamidate),[8] upon irradiation at 450 nm, shows switchable proton-dependent photoluminescence emission tunable from deep red (715 nm) to bright green (570 nm) as a function of pH. Interestingly, both complexes do not exhibit photoluminescence upon excitation either in the UV region or at the lowest absorption band, which corresponds to the HOMO−1→SOMO

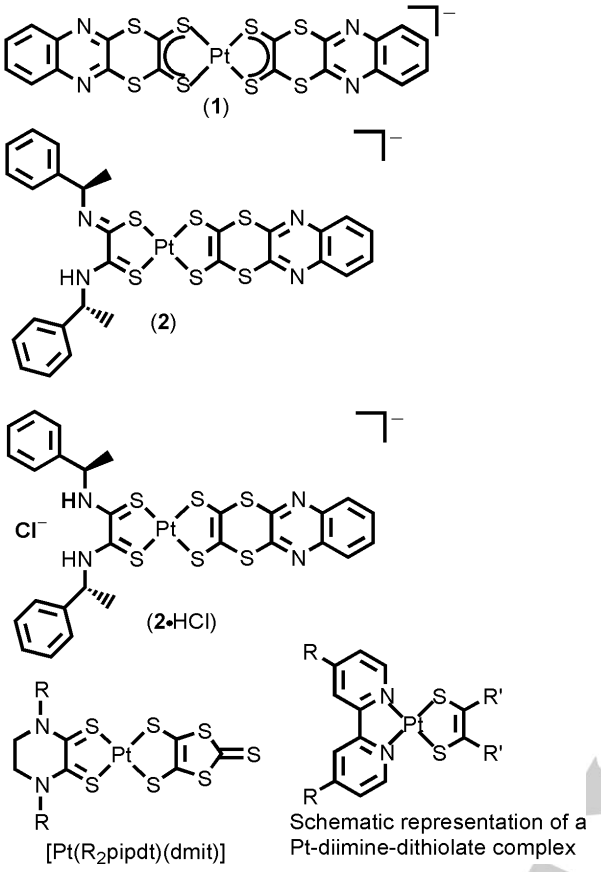

Figure 1: Homoleptic and heteroleptic Pt-dithiolene complexes. **1**, **2** and **2·HCl** exhibit luminescence in solution at RT, with apparent anti-Kasha behavior.

(homoleptic compound) and HOMO−LUMO (heteroleptic compound) transitions, respectively. The sequence of the calculated molecular orbitals suggested the intraligand charge-transfer (ILCT) nature of the process, involving orbitals of the dithiolate moiety (Quinoxdt). The RT decay times estimated in the picosecond range and the rather low quantum yields (in the 1×10^{-4} -10^{-5} range) pointed out that the radiative decay channel is strongly quenched by other deactivation pathways and that the phenomenon related to the observed spectral features can be described as an apparent "anti-Kasha" emission.

This unusual emission could be reasonably ascribed to the poor overlap between the superior Quinoxdt-based (LUMO+1) emissive state and the vicinal energy states (related to the LUMO). This orbital mismatch would promote the radiative decay from the high-energy state to the ground state to be competitive with internal conversion.

In this work we elucidate the uncommon optical behaviour of heteroleptic metal dithiolene complexes by investigating a new heteroleptic platinum-dithiolene complex, [Pt(*i*-Pr$_2$pipdt)(Quinoxdt)] (**3a**). In the design, Quinoxdt is purposely maintained, while the acceptor ligand is a neutral dithiooxamide: *i*-Pr$_2$pipdt (1,4-diisopropyl-piperazine-2,3-dithione). As discussed earlier, the similar [Pt(*i*-Pr$_2$pipdt)(dmit)] complex is not emissive, pointing to the prominent role of the Quinoxdt to the optical properties of its complexes.[3a,4a,b] For clarity reasons the cited complexes are illustrated in Figure 1. Here we report the linear and non-linear optical properties of **3a**, together with a detailed description of the electronic features as derived by density functional theory (DFT), and time-dependent DFT (TD-DFT) calculations. In order to perturb the optical features of **3a**, we have employed Ag(I) in the form of silver triflate, given the presence of a large number of potentially interacting sites on the molecular surface of **3a** with soft cations such as Ag(I). Interestingly, **3a** behaves as a cation luminescent sensor, where emission can be reversibly switched off/on in the presence/absence of Ag(I) The corresponding Ni (**3b**) and Pd (**3c**) complexes have been also prepared and investigated to assist interpretation of uncommon optical properties exhibited by **3a**.

The reactivity indices (Fukui functions)[9] pointed out the preferred interaction sites in the formation of the **3a**: Ag adduct with 1:2 ratio. Related calculated properties have been found in very good agreement with experimental findings providing new insights into the origin of the unusual optical behaviour of these complexes.

Results and Discussion

[Pt(II)(*i*-Pr$_2$pipdt)(Quinoxdt)] complex **3a** was prepared as shown in Scheme 1. Accordingly, the precursor [Pt(II)(i-Pr$_2$pipdt)(Cl$_2$)] (**4**) was added to a solution of disodium [1,4]dithiino[2,3-b]quinoxaline-2,3-bis(thiolate) (**5**), prepared *in situ* as detailed in Experimental Section. Green microcrystals of the neutral complex precipitated as the reaction proceeded. Crystals suitable for single crystal X-ray diffraction were obtained by the diffusion method using DMF as solvent and diethyl ether as anti-solvent. Palladium and nickel complexes were prepared by adapting the above procedure, as described in the Experimental Section.

The molecular structure of [Pt(*i*-Pr$_2$pipdt)(Quinoxdt)]·DMF is reported in Figure 2. The metal geometry is square planar according to the presence of four sulfur atoms from two S,S bidentate ligands. As reported for similar systems formally comprising a dithione (*i*-Pr$_2$pipdt) and a dithiolate (Quinoxdt) ligands,[3a-b, 10a-b] the metal-sulfur bond distances are in the very narrow range of 2.277(2)-2.279(2) Á, hence it is not possible to infer the electronic properties of the ligands by purely geometric

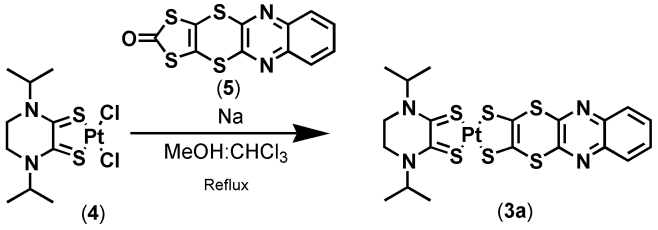

Scheme 1. Synthesis of [Pt(iPr$_2$pipdt)(Quinoxdt)].

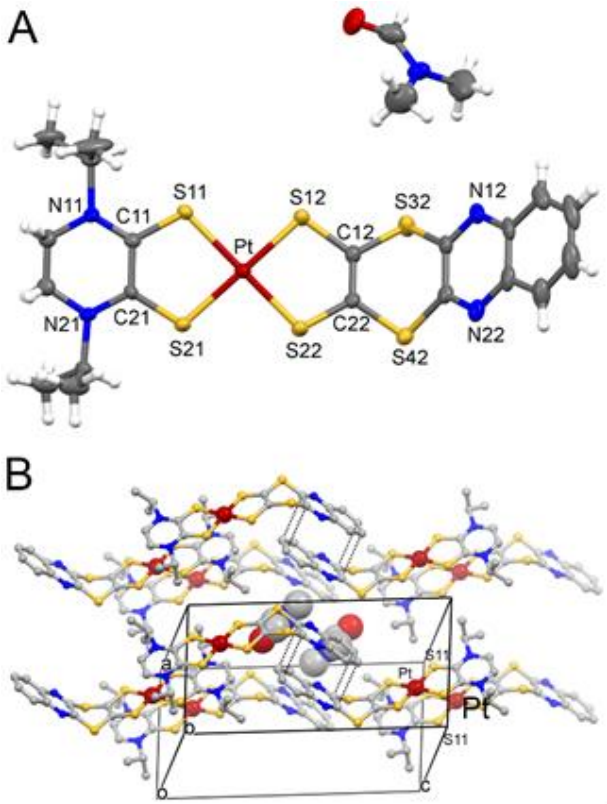

Figure 2: (a) Molecular structure of [Pt(*i*-Pr$_2$pipdt)(Quinoxdt)]·DMF (**3a**·DMF) with thermal ellipsoids drawn at the 30% probability level. (b) Portion of the crystal packing of **3a**·DMF. DMF molecules are depicted in the spacefill style. Selected geometric parameters (Å) for **3a**·DMF: Pt-S(11) = 2.279(2); Pt-S(21) = 2.278(2); Pt-S(12) = 2.279(2); Pt-S(22) = 2.277(2); C(11)-S(11) = 1.691(7); C(21)-S(21) = 1.688(7); C(12)-S(12) = 1.749(7); C(22)-S(22) = 1.743(7); C(11)-C(21) = 1.444(9); C(31)-C(41) = 1.34(1).

parameters such as the M-S bond distances. Nevertheless, the C-S bond distances in *i*-Pr$_2$pipdt (1.691(7) and 1.681(7) Å) are in agreement with a dithione structure, whereas the C-S bond distances in Quinoxdt (1.749(7) and 1.743(7) Å can be associated to a dithiolate type of structure. Likewise, the C-C bond linked to the coordinated sulfur atoms, exhibits a double bond character for the Quinoxdt (1.345(8) Å) and a single bond character for the *i*-Pr$_2$pipdt (1.444(9) Å) ligands, respectively. The crystal packing of **3a**·DMF is depicted in Figure 2b. The molecules are partially stacked with the peripheral Quinoxdt fragment forming a weakly interacting supramolecular dimer. On the other hand, the fragment comprising the metal center and the *i*-Pr$_2$pipdt ligand are marginally superimposed, with the two closest contact occurring trough the Pt and the S(11) atoms of two symmetry related molecules (3.86 Å). The DMF molecules are located into a pocket delimited by six Quinoxdt moieties and by the methyl groups four *i*-Pr$_2$pipdt residues.

The electronic absorption spectrum of **3a** in DMF solution shows two bands, one is in the vis-NIR region at 836 nm, and the second one occurs at 370 nm. An additional shoulder is found around 500 nm. The peak at lower frequency shows negative solvatochromic behaviour, as reported in Figure 3, in agreement with a decrease of the dipolar moment in the excited state. These findings are in accordance to what is generally observed in metal-d^8 heteroleptic dithione/ or diimine/dithiolate complexes, which have been largely investigated by us,[2-3,8-10] by the Eisenberg's group,[11a-b] and by others[12a-b] also for their potential use in photonics.

Table 1. Summary of X-ray crystallographic data for **3a**·DMF.

Empirical formula	$C_{23}H_{29}N_5S_6PtO$
Formula weight	778.96
Temperature/K	240(2)
Crystal system	triclinic
Space group	*P*-1
a/Å	9.017(1)
b/Å	9.237(1)
c/Å	18.037(2)
α/°	79.282(2)
β/°	86.132(2)
γ/°	72.614(2)
Volume/Å^3	1408.5(3)
Z	2
ρ_{calc}g/cm^3	1.837
μ/mm^{-1}	5.453
F(000)	768.0
Crystal size/mm^3	0.18 × 0.11 × 0.05
Radiation	MoKα (λ = 0.71073)
2Θ range for data collection/°	4.598 to 50.71
Index ranges	-10 ≤ h ≤ 10, -11 ≤ k ≤ 11, -21 ≤ l ≤ 21
Reflections collected	15616
Independent reflections	5144 [R_{int} = 0.0676, R_{sigma} = 0.0746]
Data/restraints/parameters	5144/0/331
Goodness-of-fit on F^2	1.003
Final R indexes [I>=2σ (I)]	R_1 = 0.0422, wR_2 = 0.0783 [a]
Largest diff. peak/hole / e Å^{-3}	0.61/-0.68

[a] $R1 = \Sigma||Fo|-|Fc||/\Sigma|Fo|$, $wR2 = [\Sigma[w(Fo2-Fc2)2]/\Sigma[w(Fo2)2]]^{1/2}$, $w = 1/[\sigma2(Fo2) + (aP)2 + bP]$, where $P = [\max(Fo2,0) + 2Fc2]/3$.

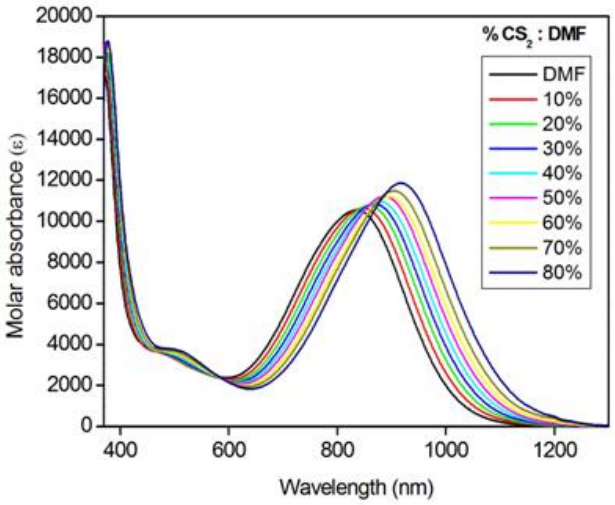

Figure 3: Solvatochromic behaviour of **3a** in DMF/CS$_2$ mixtures ranging from DMF 100% to 20%.

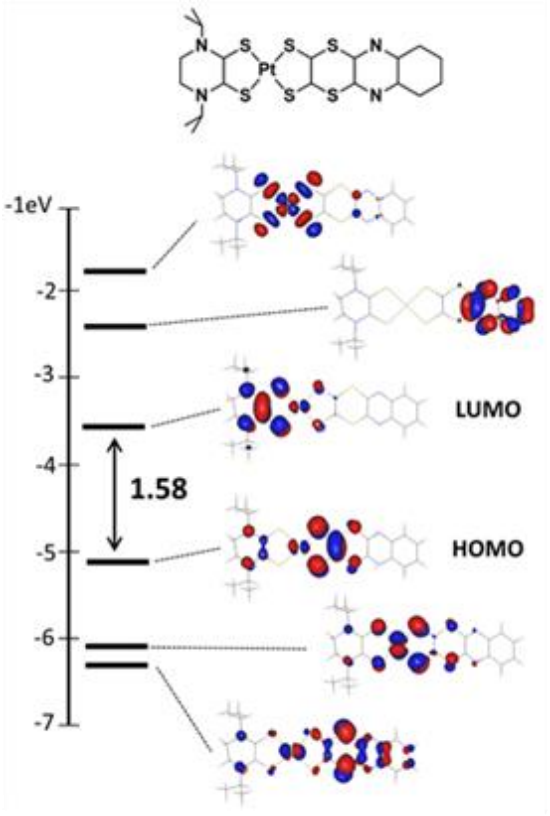

Figure 4: Frontier molecular orbitals of **3a** in the solution phase, DMF, (B3LYP/6-31+G(d)-SDD). For the DFT optimized structure see Figure S2.

The electronic structure of **3a** was investigated by means of DFT methods taking into account the solvent (DMF) by using the polarizable continuum method (PCM). The frontier orbitals are reported in Figure 4. More specifically, the HOMO and LUMO are both formed from the out-of-plane antisymmetric interactions between the metal orbital and a ligand based C2S2 orbital. The HOMO is mainly localized on the dithiolate system, whereas the LUMO is mainly localized on the dithione fragment, in agreement with previous findings for similar systems.[3] Figure 5 reports the simulated UV-vis spectrum of **3a** together with the twenty first singlet transitions responsible for the main absorption band in the visible region.

The obtained results support that the experimental band at lowest energy can be assigned to the HOMO→LUMO transition, whereas the H-2 → L+1 transition contributes to the peak centered at 370 nm, Figure 5. The band at approximately 520 nm is associated to various transitions of low intensity, but it is mainly due to the HOMO→L+1 and H-2→LUMO transitions. In more detail, and according to the shape of the frontier orbitals, the experimental band at 836 nm can be described as a metal-ligand-to-metal ligand' MMLL' CT transition from the dithiolato to the dithione ligand. The band at 370 nm is mainly of CT intraligand nature from the dithiolato moiety with some metal contribution to the periphery of Quinoxdt, whereas the band at 520 nm comprises different contributions from the three

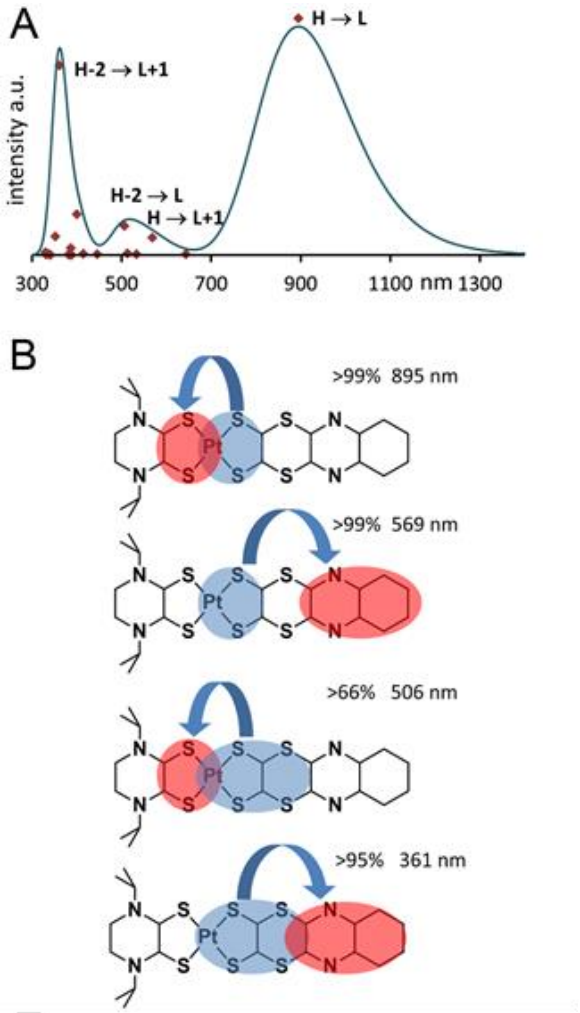

Figure 5: (A) Simulated UV-vis spectrum of **3a** together with the principal singlet transition responsible for the main absorption band in the visible region (red dots). Calculation were performed with the PCM method (DMF), B3LYP/6-31+G(d)-SDD. (B) Depiction of the molecular fragments contributions to the calculated electronic transitions.

components, metal and ligands, see Figure 5. It is worth noting that a similar sequence of MOs is found in [Pt(MBA)(Quinoxdt)]-·HCl,[8] in agreement with similar optical features in the two complexes. Interestingly, [Pt(R_2pipdt)(dmit)][3a, 10a-c] exhibits a similar HOMO-LUMO gap, in accordance with the similar wavelengths of the related absorption peaks. This observation is in line with the nature of the three complexes, since they all comprise a donor ligand (Quinoxdt or dmit) and an acceptor ligand (MBA or R_2pipdt) with very similar structure of the HOMO and LUMO orbitals as shown in Figure S3. Treatment of a solution of **3a** in DMF with increasing amount of a silver triflate solution produces a change of the absorption spectra until the 1:2 ratio between **3a** and Ag(I) is achieved, suggesting the formation of a 1:2 adduct, as shown in Figure 6. Unfortunately, any attempt to isolate and characterize the new species failed. Given the features of the absorption spectra, we tentatively suggest that the shift of the lowest energy peak to

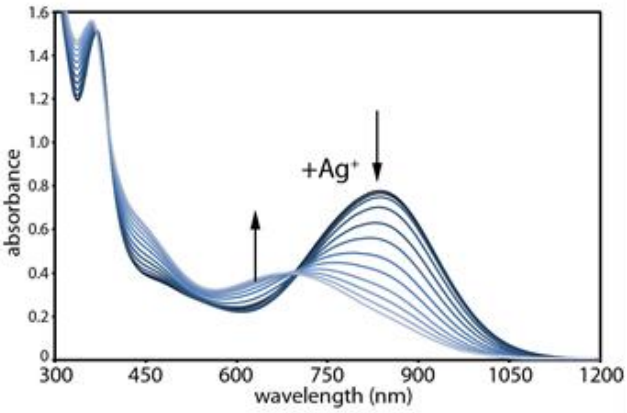

Figure 6: Variation of absorption upon successive additions of silver triflate (10 µL, $5x10^{-3}$ M) to a solution of **3a** in DMF (2.5mL, $1x10^{-4}$ M) up to a ratio 2.2:1.

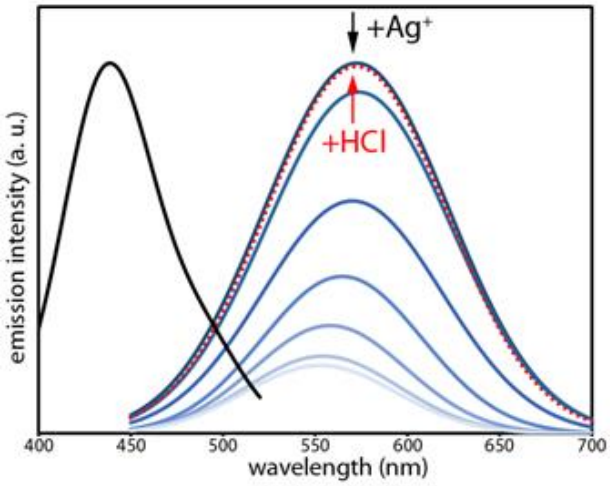

Figure 7: Variation of emission intensity of **3a** in DMF solution (2 mL, $5x10^{-4}$ M) upon successive additions of silver triflate (10 µL, $2x10^{-2}$ M) (blue lines) up to a molar ratio 1.2:1 and of HCl (100 µL, $2.5x10^{-2}$M) (red dotted line). Excitation wavelength was 440 nm. The excitation spectrum acquired by monitoring emission at 570 nm is depicted in black. Spectra for silver triflate amounts above 1.2 moles with respect to **3a** were below acceptable signal-to-noise ratio and are not reported.

lower energy reflects a stabilization of the HOMO, most likely due to an interaction of the thiolato sulphur atoms with the silver ions. It cannot be ruled out that each silver ion further interacts with thioether sulphur atoms of the heterocycle and/or with platinum (see Figures S4 and S5 for **3b** and **3c**, respectively).

As far as the emissive properties are concerned, **3a** in DMF solution shows green emission at 570 nm at room temperature upon irradiation at 440 nm, as shown in Figure 7. It is worth to note that this emission is dependent on the excitation wavelength and no photoluminescence is detected when exciting at wavelengths higher than 500 nm, according to the excitation spectrum reported in Figure 7. Moreover no emission is observed when irradiating at 750 nm in the lowest absorption band corresponding to the HOMO-LUMO transition.[13] These observations point to an apparent "anti-Kasha" behaviour similarly to what previously found for [Pt(MBA)(Quinoxdt)]·HCl**,** in agreement with the close similarity of the optical features and sequence of MOs of the two complexes (Figure S3). The low quantum yield (Φ% = 0.003) evaluated through the relative method, by using the *tris*-bipyridil ruthenium (II), $[Ru(bipy)_3]^{2+}$ as reference, point out that the radiative decay channel is however strongly quenched by other deactivation pathways, possibly through internal conversion to lower-lying energy states. With this view, it must be pointed out that the term "anti-Kasha" emission can be herein used to describe an apparent phenomenon related to the observed spectral features. Accordingly, it seems that the described behaviour provides further support to the tentative explanation that the excitation process originates mainly from ILCT transitions involving orbitals of the thiolate fragment of the Quinoxdt moiety (HOMO), and the Quinoxdt ligand periphery (LUMO+1). The analogous Ni(II) complex (**3b**) exhibits similar behaviour of **3a** (Figure S6). A different situation is found for the Pd(II) complex (**3c**) since no luminescence is observed. Also in metallo d^8 diimine dithiolato systems, Pt(II) complexes are luminescent while Pd(II) ones are typically non-emissive both in solution or in the solid state. This fact, early observed by Miller and Dance,[14] may be explained by taking into account that metal orbital energies follow the sequence: Pd >Pt≅Ni, and this can draw the energy of the Pd-$d\sigma^*$ orbital low enough to make decay through non radiative metal-centred excited states, comparable in energy to the ILCT states, so that no emission is observed. The lack of emissive properties has been observed also for Au(III) diimine dithiolato complexes, where the increased charge of the metal ion that further lowers the energy of $d\sigma^*$ orbitals, provides additional support to the involvement of non-radiative metal-centred states in the deactivation process.[15, 16]

Moreover, in the same experimental conditions, no emission was observed in the solid state for **3a-b**. The observed loss of luminescence may be ascribed to the formation of dimers partially stacked with the peripheral Quinoxdt fragment.

Interestingly, the 570 nm emission is quenched on addition of silver triflate, and is fully restored upon removal of the silver ion through HCl addition (see Figure 7). Analogous behaviour is observed for the corresponding Ni derivative **3b** (Figure S6). In order to try to find reasonable explanations to the observed features, and inspired by similar systems reported in the literature, where a d^{10} metal ion such as Au(I)[17] or Ag(I) are positioned over the Pt-S bond of heteroleptic square-planar platinum dithiolate complexes,[18] two molecular geometries that take into account the presence of Ag(I) ions close to the coordination plane (Figure S7) have been optimized. The interaction between the Ag(I) and the sulfur atom of the thiolate group can also be explained by considering the shape of the Fukui functions[19] computed for **3a**, which can provide useful information of the preferential site of interaction with an incoming electrophile or nucleophile (Figure S8). In particular, the *f*+ and *f*- functions represent the tendency that a specific fragment within a molecule can be subjected to a nucleophilic or electrophilic

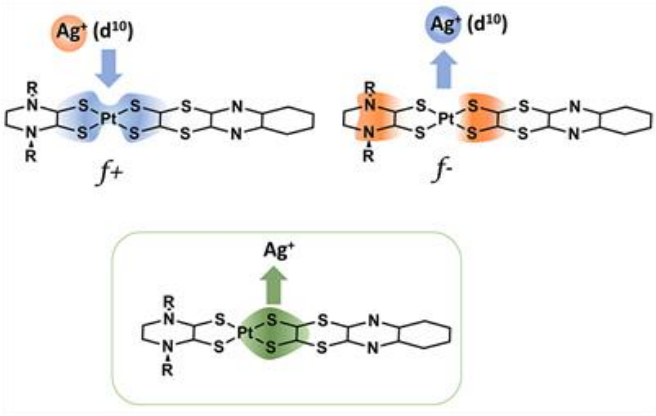

Figure 8: Preferential site of interaction of the molecular surface of **3a** and Ag(I) according to the shape of the positive and negative Fukui function *f*+ and *f*-.

attack, respectively. According to the *f*+, the atoms involved in the coordination interaction (sulfur atoms and Pt) are suitable to interact with an electron rich environment (nucleophilic attack). On the other hand, the shape of *f*- points to the N-C fragment of the dithione together with the C-S of the dithiolato ligand as potential donor groups towards an electrophile (electrophilic attack), Figure 8. Ag(I) can be regarded as a Lewis acid (electrophile) but at the same time it is a soft d^{10} species potentially acting as a nucleophile. Taking these aspects together, the best interacting site for Ag(I) can be identified with the sulfur of the thiolate group. The N atoms of the dithione can also provide a stabilizing interaction with an incoming Ag(I), but there is considerable steric hindrance deriving from the iPr residues**.** Therefore, as indicated above (see Figure S7), two molecular structures comprising two silver cations and **3a**, were considered for geometry optimization: **3a**-trans-**Ag₂** and **3a**-cis-**Ag₂**, which exhibit the two Ag-triflate fragments on the opposite side and on the same side, respectively, of the Pt coordination plane (Figure S7). The optimized adduct **3a**-trans-**Ag₂**, shown in Figure 9, shows the two silver cations in an almost linear geometry bound by a thiolate sulfur atom and a monodentate triflate anions. The molecular geometry suggests also the presence of a Pt-Ag interaction since the distances between the two metals is shorter than the van der Waals radii sum (~3.45 Å),[20] and it is close to 2.9 Å. In the optimized adduct **3a**-cis-**Ag₂**, the two silver cations exhibit a different geometry, as the compound is less symmetric than **3a**-trans-**Ag₂**. In fact, one Ag(I) shows a linear geometry and the second is in a distorted tetrahedral environment. One triflate anion is bridging between the two silver atoms (Figure S7). The computed absorption properties of the two adducts evidence a hypsochromic shift of the low energy band found at 861 nm in **3a** pointing to the role of the Ag-S/Ag-Pt interaction in modulating the absorption feature of the complex, Figure 10 and Figure S9. Nevertheless, **3a**-trans-**Ag₂** exhibits computed spectral features that are remarkably similar to the experimental findings, and this species can therefore be considered as a good model for the Ag(I)-**3a** adduct in DMF. The hypsochromic shift in **3a**-trans-**Ag₂** and **3a**-cis-**Ag₂** can be explained by a significant HOMO stabilization because of the thiolate-silver interaction. Moreover, it is worth to note that the nature of the LUMO+1 orbital is changed on interaction with silver ions. In particular, the Quinoxdt-centered MO, which is believed to be associated with the emissive properties of the compound, now occupies the LUMO+2 position in the orbital sequence, in close energy match with the LUMO+1 (Figure S10). Therefore, an additional efficient non-radiative decay channel through $d\sigma^*$ orbitals is provided, and this is in agreement with the observed luminescence quenching upon addition of silver triflate.

The collective observation of the luminescence properties of **3a-c** seem to further strength our proposal that the emissive state has ILCT (Quinoxdt) character. In fact in the Ni and Pt case similar emission wavelengths by the closely related Quinoxdt complexes (and also from the Quinoxdt ligand precursor) are observed differently to the Pt(II) diimine-dithiolato case. As said,

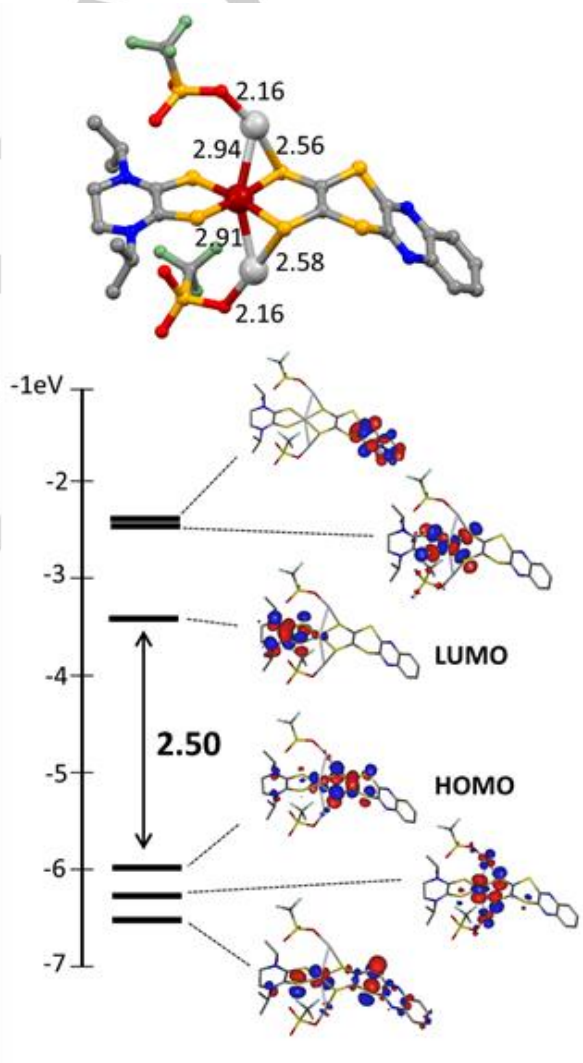

Figure 9: Above, optimized molecular structure of the adduct **3a**·2($AgCF_3SO_3$) in the gas phase (B3LYP/6-31+G(d)-SDD). Selected bond distances are reported in Å. Below, selected frontier molecular orbitals.

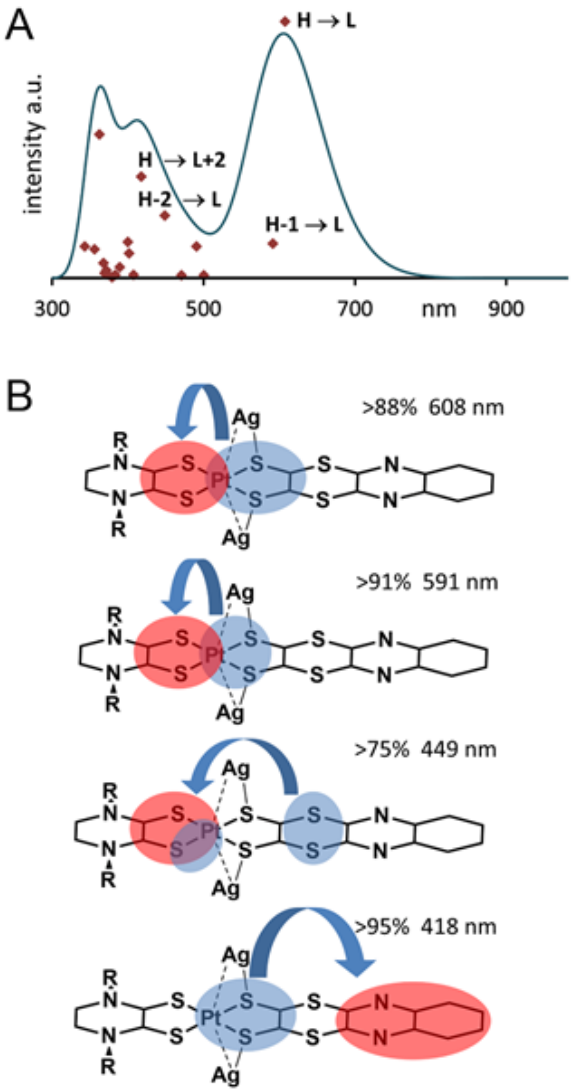

Figure 10: (A) Simulated UV-vis spectrum of the adduct **3a**·2($AgCF_3SO_3$) together with the principal singlet transition responsible for the main absorption band in the visible region (blue dots). Calculations were performed with the PCM method (DMF), B3LYP/6-31+G(d)-SDD. (B) Depiction of the molecular fragments contributions to the calculated electronic transitions.

in the Pt(II) diimine-dithiolato case the emissive state has LL' (or better MMLL') CT character and the expected trends in emission energy with ligands variation are found. Instead in heteroleptic Pt dithiolenes where the dithiolato is a heterocyclic substituted one, and the other ligand is a diphosphino derivatives, known as Pilato's systems,[21] the room temperature emissive properties are only sensitive to the changes in the heterocycle ring. A charge transfer intra ligand emissive state (dithiolato π to heterocycle π^*) has been taken responsible for their photoluminescent properties. In Pilato's systems the emissive state is the lowest one and gives rise both to fluorescence and phosphorescence (dual emission) ascribed respectively to ^{1}ILCT and ^{3}ILCT, this last quenched by oxygen.

In the case under discussion, a similar ILCT emissive state is invoked, but this state is not the lowest one. Moreover, it may be suggested that the emission is relatable to a singlet state, given it is not affected by oxygen or by changing Pt(II) with Ni(II) derivatives (a triplet state might be quenched by oxygen and should be affected by the heavy atom effect that favours the singlet-triplet intersystem-crossing mechanism).

EFISH experiments, as described in the Experimental Section, have allowed us to determine the scalar product $\mu\beta_\lambda$ (μ = ground state dipole moment; β_λ = projection of the vectorial component of the quadratic hyperpolarizability tensor along the dipole moment axis). In accordance with the negative solvatochromism and with the two-level model, the $\mu\beta_\lambda$ (10^{-48} esu) value, determined at 1907 nm incident wavelength, is negative and equal to −4280, and can be extrapolated to zero frequency by applying the equation: $\beta_0 = \beta_\lambda\,[1-(2\lambda_{max}/\lambda)^2][1-(\lambda_{max}/\lambda)^2]$ giving for $\mu\beta_0$(10^{-48} esu) the value −742. The $\mu\beta_\lambda$ values for **3b** and **3c** are –1490 and –1970 ×10^{-48} esu, respectively, significantly lower than for the Pt(II) derivative **3a**, in agreement with expectations. When comparing these values with those determined for similar compounds [M(R_2pipdt)(dmit)]: M = Pt, $\mu\beta_\lambda$ = –10000 R = Bz and –7300 R = iPr; M = Ni, $\mu\beta_\lambda$ = –6100 R = Bz, –6200 R = iPr; M = Pd, $\mu\beta_\lambda$ = –5360 R = Bz, –4700 R = iPr [3b, 10b] we observe that the expected sequence of values (Pt > Ni > Pd) is maintained, but the $\mu\beta_\lambda$ values are lower. The largest molecular hyperpolarizability of dmit derivatives, among the highest values so far reported for metal complexes, may be explained through the relationship $\beta \propto (\mu_\gamma - \mu_\varepsilon)(\mu_{\gamma\varepsilon})^2/(E_{\mu\alpha\xi})^2$ proposed by Oudar et al. taking into account a simplified two-state model[22, 23] where μ_e and μ_g are the excited state and the ground state dipole moments, respectively, μ_{ge} is the transition state dipole moment, and ΔE_{ge} is the transition energy between the two states. It has been shown that structural changes affect the electronic properties of these complexes since the worse the overlap between the orbitals that contribute to the final states, the lower the oscillator strength (relatable to the transition state dipole moment) of the main CT band.[3a] In the cases under discussion the most significant difference between the complexes appears to derive from the differences in the oscillator strength of the main charge-transfer band, which is larger in the dmit derivative (*f* = 0.45 for R = Bz *versus* 0.35 for **3a**). This can be explained by taking into account that the π-orbital system that contributes to the final states is extended to the periphery of the ligand in the dmit, while it is interrupted by the presence of thio-ether bridges in Quinoxdt.

It is worth to note that **3a**-**c** have a higher transparency window in the visible region with respect to corresponding dmit derivatives, which show a medium strong absorption band near 500nm relatable to a highly mixed transition which includes the HOMO-LUMO+1 one.

Conclusions

This work provides a rational synthesis and deep understanding of the factors which affect the properties of heteroleptic d^8 metallodithiolene compounds with potential as smart optical

materials with tunable emission and NLO properties. In this report, we have detailed the synthesis and physical characterization of the [Pt(i-Pr_2pipdt)(Quinoxdt)] complex (**3a**) and of the corresponding Ni and Pd derivatives inside the triad. These complexes**,** characterized by the presence of an acceptor and a donor ligands at the opposite side of the M(II) center, show negative solvatochromic absorption and high second-order polarizability relatable to CT donor-acceptor transition**. 3a** shows uncommon room temperature emission. In fact, after the excitation at 440 nm, the observed emission is found at 570 nm, which is significantly higher in energy than the low-energy absorption (836 nm). This process is in line with a potential anti-Kasha behaviour of the complexes. Addition of silver triflate produces the formation of a **3a**:Ag(I) 1:2 adduct, with significant change of the optical properties, that is hypsochromic shift of the lowest absorption band, and quenching of the green "anti-Kasha" luminescence at 570 nm. After silver removal, the initial luminescence is restored. Similar behaviour is observed for the corresponding Ni(II) derivative while the Pd(II) one is non-emissive. Computational studies have provided a crucial contribution to support the interpretation of the observed properties. The Fukui functions indicated the preferential sites of interaction with incoming electrophile or nucleophile, and in particular with a soft metal ion such as Ag(I). According to these computations, the thiolic sulfur atoms and to a minor extent the Pt center are the preferential sites of interaction with the silver ions. In addition, the comparison of the properties of **3a** with those of [Pt(i-Pr_2pipdt)(dmit)], and of [Pt(MBA)(Quinoxdt)]$^{-}$·HCl shows that all the complexes exhibit high second order NLO activity, but only those which bear the Quinoxdt ligand emit with an apparent "anti-Kasha" behaviour. MOs sequence in non-emitting complexes (including silver adduct of **3a**) shows that the metal-centered $d\sigma^*$ orbital is lowered in energy with respect to the π^* ligand orbital, likely providing an efficient non-radiative *d-d* decay channel.[16]

Collective observations supported by computational studies enabled us to shed light on the steric-electronic influence of substituted dithiolene ligands (R, R = Quinoxdt) on the relevant optical properties, such as the unique emission behaviour of this class of complexes.

Experimental Section

Synthesis. Reagents and solvents were purchased from Aldrich and used without further purification. Complex **4** was prepared following ref. 3b and ligand **5** was prepared according to ref. 24.

[Pt(iPr_2pipdt)(Quinoxdt)] (3a): A solution of sodium (7.9 mg, 3.46 mmol) in 10mL of methanol was added to a suspension of **5** (48.5 mg, 1.57 mmol) in 50% MeOH/$CHCl_3$ mixture and stirred at room temperature for 30 minutes. The brown solution of dithiolate formed was added drop-wise to a reddish solution of **4** (78 mg, 1.57 mmol) in 200mL of 15% MeOH/$CHCl_3$. The reaction mixture was then refluxed overnight to obtain green microcrystalline [Pt(i-Pr_2Pipdt)(Quinoxdt)] (**3a**) (96mg, 86%) which was collected by centrifugation followed by washing with diethyl ether. Well-formed crystals suitable for single crystal XRD studies were obtained through re-crystallization by diffusion from DMF/diethyl ether. UV-vis (DMF solution): λ (nm) ε (mol cm^{-1} dm^{-3}): 369 (1.73×10^4); 465sh (3.8×10^3); 836 (1.05×10^4). FT–IR: ν_{max} cm^{-1}: 3106 (vw); 3062 (vw); 2930 (w); 2858 (w); 1664–1609 (s-ms), νCO DMF; 1503 (s), νCN *i*-Prpipdt; 1357 (ms), νCC quinoxdt; 1264 (ms); 1177 (s); 1111 (vs); 1050 (ms); 959 (m); 854 (ms); 762 (s); 658 (m); 597 (s). ^{1}H NMR [$(CD_3)_2SO$] δ: 7.96 (CH, 1H,s DMF); 7.90 (CH, 2H m) 7.75 (CH 2H m); 5.15 (CH 1H m), 4.92 (CH 1H m); 3.75 (CH_2 2H s); 2.89-2.73 (CH_3 3H s - CH_3 3Hs DMF); 1.48 (CH_3) 6H d 1.35 (CH_3) 6H d (the other signal of the CH_2 protons of the pip ring is likely covered by the peak at 3.25-3.35 ppm arising from water). Peaks at 1.1 (CH_3), 1 H t, and 3.4 CH_2, 0.8 H q, shows the presence of adsorbed Et_2O). XRD patterns of **3a** powders are consistent with single crystal data of **3a** as shown in Figure S11.

Measurements

IR spectra (4000−400 cm^{-1}) were recorded with a Bruker Tensor 27 Platinum ATR. ^{1}H-NMR spectra were performed on Bruker 500 MHz at room temperature. Electronic absorption spectra were recorded with an Agilent Cary 5000 spectrophotometer. X-ray Powder Diffraction measurements were performed on a Panalytical Empyrean diffractometer equipped with a graphite monochromator on the diffracted beam and an X'Celerator linear detector. The scans were collected under spinning at 1 Hz within the range of 4°-80° (2θ) using CuKα radiation

Experimental single crystal X-ray

A summary of data collection and structure refinement for [Pt(i-Pr_2pipdt)(quinoxdt)]·DMF is reported in Table 1. Single crystal data were collected with a *Bruker Smart APEXII* at 240 K (Mo Kα, λ = 0.71073 Å). The intensity data were integrated from several series of exposures frames (0.3° width) covering the sphere of reciprocal space.[25] Absorption correction were applied using the program SADABS.[26] The structures were solved by the dual space algorithm implemented in the SHELXT code.[27] Fourier analysis and refinement were performed by the full-matrix least-squares methods based on F2 implemented in SHELXL-2014.[28] Graphical material was prepared with the Mercury 3.9 program.[29] CCDC 1833235 contains the supplementary crystallographic data for this paper.

Computational studies

The electronic properties of [Pt(i-Pr_2pipdt)(quinoxdt)] were investigated by means of DFT methods.[30] The molecular structure of the complex was optimized starting from the experimental geometry derived by the X-ray structural characterization using no symmetry constraints. The Becke three-parameter exchange functional with Lee-Yang-Parr correlation functional (B3LYP)[31, 32] was employed together with the 6-31+G(d,) basis set for the C, H, N, and S atoms.[33, 34] The Pt atom was treated and SDD valence basis set[35, 36, 37] and with the MWB60 effective core potentials in order to take into account relativistic effects. To address acetonitrile solvation effects, the polarisable continuum model (PCM) was applied during the single point calculations using gas-phase optimized geometries.[38] The first twenty singlet-singlet vertical excitation energies of [Pt(i-Pr_2pipdt)(quinoxdt)] were determined using time-dependent density functional theory (TD-DFT).[39, 40] Also for these calculations, the contribution of the solvent was taken into account by the PCM method. The dipole moment difference between the excited and ground states ($\Delta\mu_{ge}$ = −6.9 Debye) was calculated by using the finite field approach (external field strength of ±0.001 atomic units). Fukui functions[9, 19, 41] were computed by taking the difference of the electron density of the N+1 and N system, $f+=\rho(N+1)-\rho(N)$, and the difference between the electron density of the N and N-1 system, $f- =\rho(N)-\rho(N-1)$ (N = number of electrons) using the optimized geometry of the neutral species (N). All the calculations were performed with the Gaussian 03 program suite.[42]

Molecular orbital diagrams and isodensity surfaces were generated with the Gabedit program.[43] AOMix was used to analyzed the electronic transitions obtained from TD-DFT calculations.[44]

Photoluminescence studies.

Emission spectra were collected with a Horiba-Jobin Yvon Fluoromax-4 Spectrofluorimeter using a 400W Xenon lamp. All spectra were corrected for detector response. Appropriate optical filters were used. Band pass was set as 10 nm slit width for each measurement. Solvent contribution was subtracted for all absorbance/emission spectra. Emission quantum yield was evaluated using the relative method though the following equation:

$$\Phi = \Phi_R \times (a_R/a) \times (I/I_R) \times (n/n_R)^2$$

where the R index refers to the photoluminescence standard. Φ_R= reference quantum yield; $a_R=1-10^{-AR}$, absorption factor of the reference at excitation wavelength; $a=1-10^{-A}$, absorption factor of the sample at excitation wavelength; A_R=absorbance of the reference at excitation wavelength; A=absorbance of the sample at excitation wavelength; I=sample integrated emission; I_R=reference integrated emission; n=refractive index of the medium. $[Ru(bpy)_3]^{2+}$ was used as suitable reference standard.

Second-order Nonlinear Optical Properties

The second order NLO responses of the molecular chromophore was measured by the EFISH (Electric Field Induced Second Harmonic generation) technique, which provides the γ_{EFISH} value, from which EFISH quadratic hyperpolarizability β_λ can be obtained through eq. 1

$$\gamma_{EFISH} = (\mu\beta_\lambda/5KT) + \gamma(-2\omega;\omega,\omega,0) \quad (1)$$

where μ is the ground state dipole moment, $\mu\beta_\lambda/5KT$ the dipolar orientational contribution, λ is the fundamental wavelength of the incident photons in the EFISH experiment, $\gamma(-2\omega;\omega, \omega, 0)$ is a third-order term at frequency ω of the incident photons, corresponding to the cubic contribution to γ_{EFISH}, usually negligible for dipolar chromophores such as this studied in this work. Finally, β_λ is the projection along the dipole moment axis of the vectorial component β_{VEC} of the tensorial quadratic hyperpolarizability. In the following β_λ is reported as β_{1907} since the EFISH experiments were carried out working with a 1907 nm non resonant incident wavelength. All the EFISH measurements were carried out in DMF solutions at 10^{-3} M concentration and the experimental $\mu\beta_{1907}$ values obtained are the averages of 16 measurements. All experimental EFISH $\mu\beta_{1907}$ values are defined according to the "phenomenological" convention.[45]

Acknowledgements

Università degli Studi di Cagliari and Regione Autonoma della Sardegna are acknowledged for supporting this research through Premialità PRIN 2016. The authors are grateful to Dr Flaminia Cesare Marincola for NMR spectra. F.A. gratefully acknowledges the Research Foundation Flanders (FWO) and the European Union's Horizon 2020 research and innovation programme for a Marie Skłodowska-Curie grant, agreement No 665501.

Keywords: Dithiolenes• Optical Properties • Crystal Structure • DFT calculations • Platinum

[1] a) A. Das, Z. Han, W. W. Brennessel, P. L. Holland, R. Eisenberg, *ACS Catalysis* **2015**, *5*, 1397-1406; b) R. Kato, *Chem. Rev.* **2004**, *104*, 5319–5346; c) G. C. Anyfantis, G. C. Papavassiliou, N. Assimomytis, A. Terzis, V. Psycharis, C. P. Raptopoulou, P. Kyritsis, V. Thoma, I. B. Koutselas, *Solid State Sciences* **2008**, *10*, 1729-1733.

[2] P. Deplano, D. Espa, M. L. Mercuri, L. Pilia, A. Serpe, *Coord. Chem. Rev.* **2010**, *254*, 1434–1447.

[3] a) D. Espa, L. Pilia, C. Makedonas, L. Marchiò, M. L. Mercuri, A. Serpe, A. Barsella, A. Fort, C. A. Mitsopoulou, P. Deplano, *Inorg. Chem.* **2014**, *53*, 1170−1183; b) D. Espa, L. Pilia, L. Marchio, M. L. Mercuri, A. Serpe, A. Barsella, A. Fort, S. J. Dalgleish, N. Robertson, P. Deplano, *Inorg.Chem.* **2011**, *50*, 2058−2060.

[4] a) A. Iuris, P. Deplano et al. unpublished results; b) F. Frei, A. Rondi, D. Espa, M. L. Mercuri, L. Pilia, A. Serpe, A. Odeh, F. Van Mourik, M. Chergui, T. Feurer, P. Deplano, A. Vlček, Jr., A. Cannizzo, *Dalton Trans.* **2014**, *43*, 17666–17676.

[5] M. Hissler, J. E. McGarrah, W. B. Connick, D. K. Geiger, S. D. Cummings, R. Eisenberg, *Coord. Chem. Rev.* **2000**, *208*, 115.

[6] M. Kasha, *Discuss. Faraday Soc*. **1950**, *9*, 14−19.

[7] S. Attar, D. Espa, F. Artizzu, M. L. Mercuri, A. Serpe, E. Sessini, G. Concas, F. Congiu, L. Marchiò, P. Deplano, *Inorg. Chem.* **2016**, *55*, 5118-26.

[8] S. Attar, D. Espa, F. Artizzu, L. Pilia, A. Serpe, M. Pizzotti, G. Di Carlo, L. Marchiò, P. Deplano, *Inorg. Chem.* **2017**, *56*, 6763−6767.

[9] R. G. Parr, W. Yang, *J. Am. Chem. Soc.* **1984**, *106*, 4049-4050.

[10] a) D. Espa, L. Pilia, L. Marchiò, F. Artizzu, A. Serpe, M. L. Mercuri, D. Simão, M. Almeida, M. Pizzotti, F. Tessore, P. Deplano, *Dalton Trans.*, **2012**, *41*, 3485-3493; b) L. Pilia, D. Espa, A. Barsella, A. Fort, C. Makedonas, L. Marchiò, M. L. Mercuri, A. Serpe, C. A. Mitsopoulou, P. Deplano, *Inorg. Chem.* **2011**, *50*, 10015–10027; c) D. Espa, L. Pilia, L. Marchiò, S. S. Attar, A. Barsella, A. Fort, M. L. Mercuri, A. Serpe, P. Deplano, *CrystEngComm* **2015**,*17,* 4161-4171.

[11] a) S. D. Cummings, R. Eisenberg, *J. Am. Chem. Soc.* **1996**, *118*, 1949-1960; b) S. D. Cummings, L.-T. Cheng, R. Eisenberg, *Chem. Mater.* **1997**, *9*, 440-450.

[12] a) C. Mitsopolou, *Coord. Chem. Rev.* **2010**, *254*, 1448-1456; b) E. A. M. Geary, L. J. Yellowlees, L. A. Jack, I. D. H. Oswald, S. Parsons, N. Hirata, j. R. Durrant, N. Robertson, *Inorg. Chem*. **2005**, *44*, 242-250.

[13] Although spectral range instrumental limits may hamper the direct observation of emission in the near-infrared region (>850 nm) in this case, we can compare the spectral properties with those the analogous compound **2**. In the latter, the lowest-lying absorption band falls below 600 nm and allows photoluminescence investigation up to the near-infrared (~900 nm) without the interference of inner filter effects (mainly due to re-absorption). The absence of any detectable emission in the near-infrared following excitation in the lowest HOMO-LUMO band in **2**, provides, by analogy, further support to the apparent anti-Kasha behaviour of **3a**.

[14] T. R. Miller, G. Dance, *J. Am. Chem. Soc.* **1973**, *95*, 6970.

[15] M. A. Mansour, R. J. Lachicotte, H. J. Gysling, R. Eisenberg, *Inorg. Chem.* **1998**, *37*, 4625.

[16] S. D. Cummings, R. Eisenberg in *Dithiolene Chemistry: synthesis, Properties and Applications, Progress in Inorganic Chemistry*, Vol. 52 (Eds.: E. I. Stiefel, John Wiley & Sons, Inc), **2004**, pp. 316-367.

[17] F. Juliá, P. Jones, P. González-Herrero, *Inorg Chem* **2012**, *51*, 5037.

[18] J. Moussa, L.M. Chamoreau M.P. Gullo, A. Degli Esposti; A. Barbieri, H. Amouri, *Dalton Trans*, **2016**, *45*, 2906.

[19] Chemical Reactivity Theory: A Density Functional View, CRC press, 2009, Ed. P. K. Chattaraj

[20] S. S. Batsanov, *Inorganic Materials*, **2001**, *37*, 871–885.

[21] R. S. Pilato, K. A. Van Houten in *Dithiolene Chemistry: synthesis, Properties and Applications, Progress in Inorganic Chemistry*, *Vol. 52*, (Eds.: E. I. Stiefel, John Wiley & Sons, Inc) **2004,** pp. 369-397.

[22] J. L. Oudar, D. S. Chemla, *J. Chem. Phys.* **1997**, *66*, 2664.
[23] S. Bruni, E. Cariati, F. Cariati, F. A. Porta, S. Quici, D. Roberto, *Spectrochim. Acta, Part A*, **2011**, *57*, 1417–1426.
[24] L. Hu, J. Qin, N. Zhou, Y.-F. Meng, Y. Xu, J.-L. Zuo, X.-Z. You, *Dyes Pigm*. **2012**, *92*, 1223.
[25] (SMART (control) and SAINT (integration) software for CCD systems; Bruker AXS: Madison, WI, 1994)
[26] (Area-Detector Absorption Correction; Siemens Industrial Automation, Inc.: Madison, WI, 1996
[27] G. M. Sheldrick, *Acta Crystallographica Section A*, **2005**, *71*, 3-8
[28] G. M. Sheldrick, *Acta Crystallographica Section C*, **2005**, *71*, 3-8.
[29] C. F. Macrae, P. R. Edgington, P. McCabe, E. Pidcock, G. P. Shields, R. Taylor, M. Towler, J. J. van de Streek, *Appl. Crystallogr.* **2006**, *39*, 453-457.
[30] R. G. Parr, W. Yang in *Density-Functional Theory of Atoms and Molecules*, (Ed. Oxford University Press), New York, **1989**.
[31] A. D. Becke, *Physical Review A: Atomic, Molecular, and Optical Physics*, **1988**, *38*, 3098-3100.
[32] A. D. Becke, *Journal of Chemical Physics* **1993**, *98*, 5648-5652.
[33] R. Ditchfield, W. J. Hehre, J. A. Pople, *J. Chem. Phys.* **1971**, *54*, 724.
[34] V. A. Rassolov, M. A. Ratner, J. A. Pople, P. C. Redfern, L. A. Curtiss, *J. Comp. Chem.* **2001**, *22*, 976.
[35] P. Fuentealba, H. Preuss, H. Stoll, L. v. Szentpaly, *Chem. Phys. Lett*. **1989**, *89*, 418.
[36] X. Y. Cao, M. Dolg, *J. Mol. Struct. (Theochem)* **2002**, *581*, 139.
[37] P. Schwerdtfeger, M. Dolg, W. H. E. Schwarz, G. A. Bowmaker, P. D. W. Boyd, *J. Chem. Phys.* **1989**, *91*, 1762.
[38] B. Mennucci, J. Tomasi, *J. Chem. Phys.* **1997**, *106*, 5151.
[39] M. E. Casida, C. Jamorski, K. C. Casida, D. R. Salahub, *Journal of Chemical Physics* **1998**, *108*, 4439-4449.
[40] R. E. Stratmann, G. E. Scuseria, M. J. Frisch, *Journal of Chemical Physics* **1998**, *109*, 8218-8224.
[41] K. Fukui, *Science* **1982**, *218*, 747-784.
[42] Gaussian 03, Revision C.02, M. J. Frisch, g. W. Trucks, H. B. Schlegel, G. E. Scuseria, M. A. Robb, J. R. Cheeseman, Jr, J. A. Montgomery, T. Vreven, K. N. Kudin, J. C. Burant, J. M. Millam, S. S. Iyengar, J. Tomasi, V. Barone, B. Mennucci, M. Cossi, G. Scalmani, N. Rega, G. A. Petersson, H. Nakatsuji, M. Hada, M. Ehara, K. Toyota, R. Fukuda, J. Hasegawa, M. Ishida, T. Nakajima, Y. Honda, O. Kitao, H. Nakai, M. Klene, X. Li, J. E. Knox, H. P. Hratchian, J. B. Cross, V. Bakken, C. Adamo, J. Jaramillo, R. Gomperts, R. E. Stratmann, O. Yazyev, A. J. Austin, R. Cammi, C. Pomelli, J. W. Ochterski, P. Y. Ayala, K. Morokuma, G. A. Voth, P. Salvador, J. J. Dannenberg, V. G. Zakrzewski, S. Dapprich, A. D. Daniels, M. C. Strain, O. Farkas, D. K. Malick, A. D. Rabuck, K. Raghavachari, J. B. Foresman, J. V. Ortiz, Q. Cui, A. G. Baboul, S. Clifford, J. Cioslowski, B. B. Stefanov, G. Liu, A. Liashenko, P. Piskorz, I. Komaromi, R. L. Martin, D. J. Fox, T. Keith, M. A. Al-Laham, C. Y. Peng, A. Nanayakkara, M. Challacombe, P. M. W. Gill, B. Johnson, W. Chen, M. W. Wong, C. Gonzalez, J. A. Pople, Gaussian, Inc., Wallingford CT, **2004**
[43] A. R. Allouche, *Journal of Computational Chemistry* **2011**, *32*, 174-182.
[44] S. I. Gorelsky, AOMix: Program for Molecular Orbital Analysis, http://www.sg-chem.net/, version 6.52, **2011**.
[45] A. Willetts, J. E. Rice, D. M. Burland, D. P. Shelton, *J.Chem.Phys.* **1992**, *97*, 7590-7599.

Entry for the Table of Contents

FULL PAPER

The uncommon optical properties of the depicted compound: apparent anti-Kasha emission, switchable for silver addition/removal, and 2nd NLO activity, are elucidated here by combined experimental and theoretical studies.

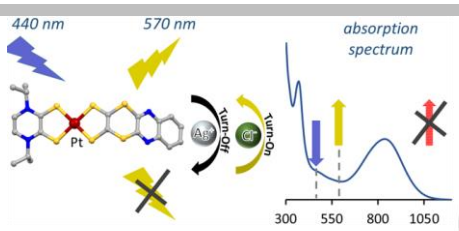

Salahuddin S. Attar, Flavia Artizzu, Luciano Marchiò, Davide Espa, Luca Pilia, Maria F. Casula, Angela Serpe, Maddalena Pizzotti, Alessio Orbelli Biroli and Paola Deplano**

Page No. – Page No.

Uncommon Optical Properties and Silver-responsive Turn-off/on Luminescence in a Pt(II) heteroleptic dithiolene complex.

Uncommon Optical Properties and Silver-responsive Turn-off/on Luminescence in a Pt(II) heteroleptic dithiolene complex

Salahuddin S. Attar,[a] Flavia Artizzu,[b] Luciano Marchiò,[c] Davide Espa,[a] Luca Pilia,[d] Maria F. Casula,[a] Angela Serpe,[e] Maddalena Pizzotti,[f] Alessio Orbelli Biroli[g] and Paola Deplano[a]

Supplementary Material

[a]*Department of Chemical and Soil Sciences, University of Cagliari, INSTM Research Unit, 09042 Monserrato (CA), Italy.*

[b]*L^3 – Luminescent Lanthanide Lab, Department of Chemistry, Ghent University, Krijgslaan 281 – building S3, B-9000 Gent, Belgium*

[c] *Dipartimento di Scienze Chimiche, della Vita e della Sostenibilità Ambientale, Università di Parma, Parco Area delle Scienze 11/a, 43124 Parma, Italy.*

[d]*Dipartimento di Ingegneria Meccanica, Chimica e dei Materiali, Università di Cagliari, Via Marengo 2, 09123 Cagliari, Italy.*

[e] *Dipartimento di Ingegneria Civile, Ambientale e Architettura, Università di Cagliari, Via Marengo 2, 09123 Cagliari, Italy.*

[f]*Department of Chemistry, University of Milan, INSTM Research Unit, Via C. Golgi 19, 20133 Milano, Italy*

[g]*Istituto di Scienze e Tecnologie Molecolari del CNR (CNR-ISTM), SmartMatLab Centre, Via C. Golgi 19, 20133 Milano, Italy*

Synthesis and characterization of complexes 3b and 3c

[Ni(iPr$_2$pipdt)(Quinoxdt)] (3b): a solution of $NiCl_2.6H_2O$ (77.4 mg, 3.26 mmol) in 10 ml of methanol was added to a stirring solution of iPr$_2$pipdt ligand (75mg, 3.26 mmol) in 100 mL 50% MeOH:$CHCl_3$ the reaction mixture was then refluxed for 2 hrs to obtain a blue-green solution. A solution of dithiolate obtained as described for **3a** from **5** (100.4mg, 3.26 mmol) was added to the reaction mixture and then refluxed overnight. The reaction mixture was concentrated to 1/4th, centrifugated and washed with ethanol and with diethyl ether obtaining a green precipitate corresponding to [Ni(i-Pr$_2$Pipdt)(Quinoxdt)] (102mg, yield 55%). Recrystallization was carried out in DMF/diethyl ether by diffusion obtaining [Ni(i-Pr$_2$Pipdt)(Quinoxdt)]DMF in form of microcrystals. UV-vis (DMF solution): λ (nm) ε (mol cm^{-1}dm^{-3}): 354 (1.3×10^4); 526sh (2.1×10^3); 863 (8×10^3). FT–IR: ν_{max} cm^{-1}: 3069 (broad); 2977 (w); 2925 (m); 1670 (m, νCO DMF) 1616 (ms); 1509 (ms,νCN Prpipdt); 1358(ms, νCC quinoxdt); 1262 (ms), 1182 (s), 1112 (vs); 1014 (vw), 961 (m); 872 (m); 767 (s); 731 (ms); 661 (w), 590 (s).

[Pd(iPr$_2$pipdt)(Quinoxdt)] (3c): this complex has been prepared similarly to **3a**. Accordingly, a dark brown solution of dithiolate prepared from **5** (103mg, 3.33mmol) was added to a solution of [Pd(iPr$_2$pipdt)DMSO.Cl] (150mg, 3.33 mmol) in 50% MeOH:$CHCl_3$ and the mixture was refluxed overnight to obtain dark brown powder of [Pd(i-Pr$_2$Pipdt)(Quinoxdt)] (172mg 83%) which was collected by centrifugation. Recrystallization was carried out in DMF/diethyl ether by diffusion. UV-vis (DMF solution): λ (nm) ε (mol cm^{-1} dm^{-3}): 368 (2.18×10^4); 773 (3.8×10^3). FT–IR: ν_{max} cm^{-1}: 3100 (broad); 2930 (w), 2854 (w); 1660–1607 (ms-m), νCO DMF, 1501 (ms), νCN i-Pr2pipdt; 1359 (ms) νCC quinoxdt; 1266 (ms); 1204 w; 1173 (s); 1120 (vs); 951 (w); 863 (m); 758 (s); 600 (s)

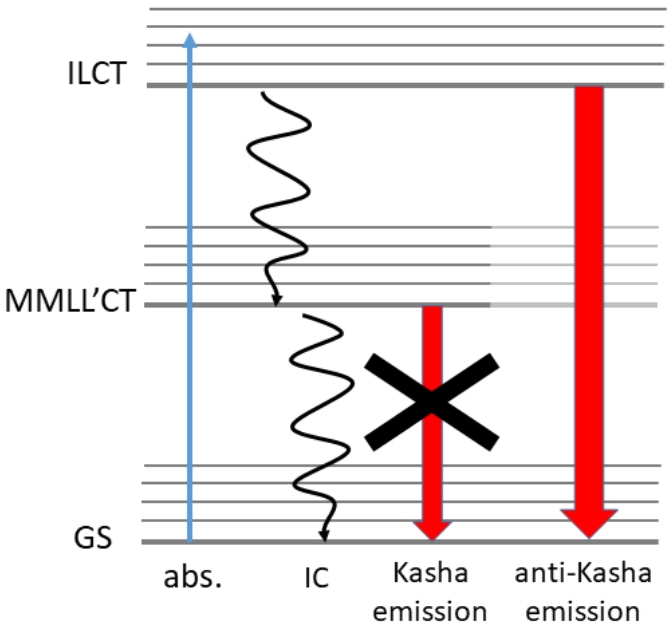

Figure S1. Proposed general scheme for the anti-Kasha emissive behavior in complexes **1-3**. Absorption (abs.) in the UV-vis region promotes a transition of high intra-ligand charge transfer (ILCT) character (see text). The excited state then relaxes by a multi-step internal conversion (IC) process through the low-lying excited MMLL'CT state or in a radiative way directly to the ground state (GS) giving rise to anti-Kasha luminescence. No "Kasha emission" from the first MMLL'CT excited state is observed in these systems.

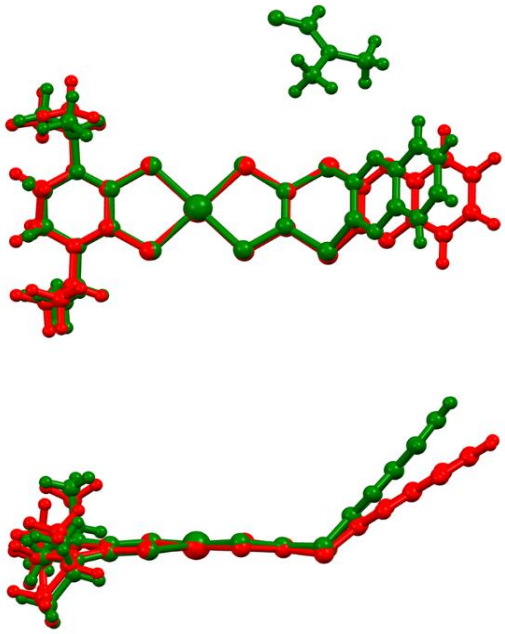

Figure S2. Superposition of the X-ray molecular structure (green) and of the DFT optimized structure of **3a** (red). B3LYP/6-31+G(d)-SDD. The main differences are in the coordination bond lengths, which are slightly overestimated by the calculations (~0.04 Å), and in the greater dihedral angle between the peripheral quinoxdt and metal coordination planes in the optimized structure with respect to the experimental geometry.

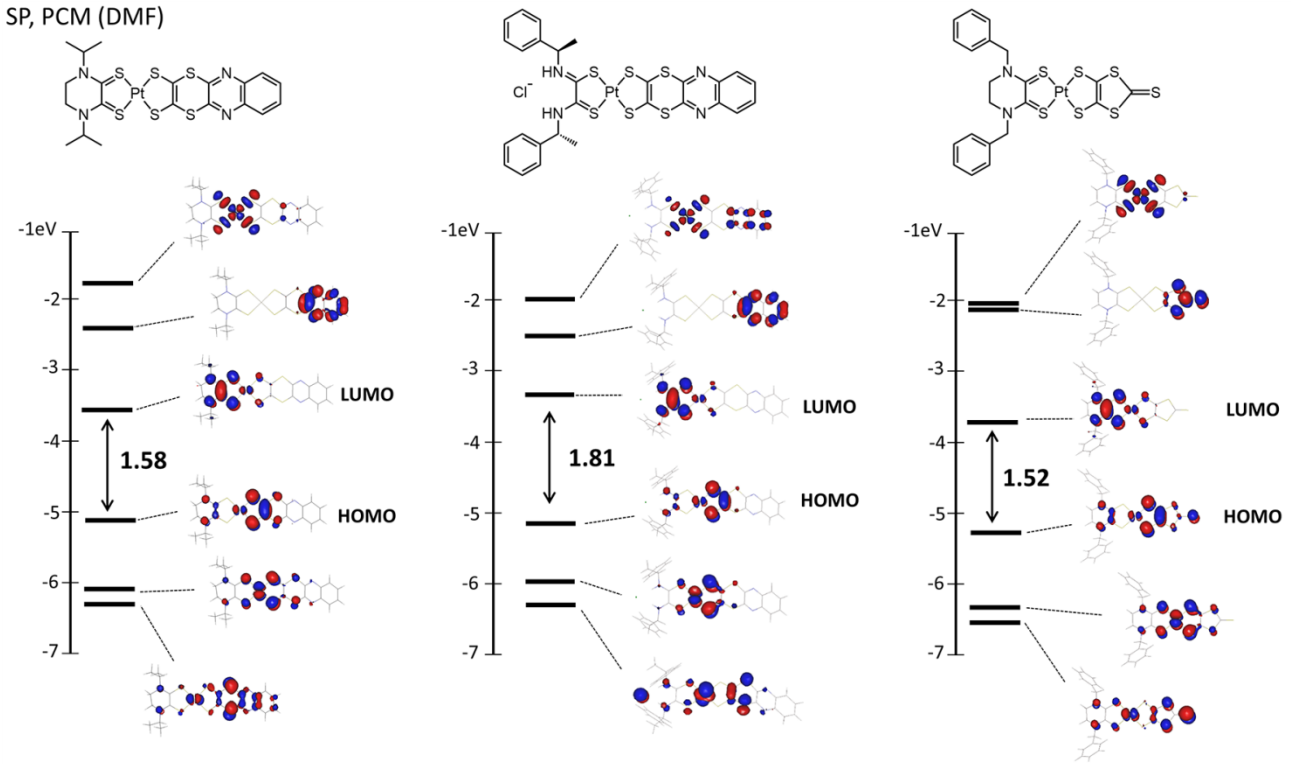

Figure S3. Comparison of the molecular orbitals of the complexes [Pt(i-Pr$_2$pipdt)(dmit)], [Pt(MBA)(Quinoxdt)]$^-$·HCl, and [Pt(i-Pr$_2$pipdt)(Quinoxdt)]. B3LYP/6-31+G(d)-SDD. Computation were performed with the PCM method using DMF as solvent.

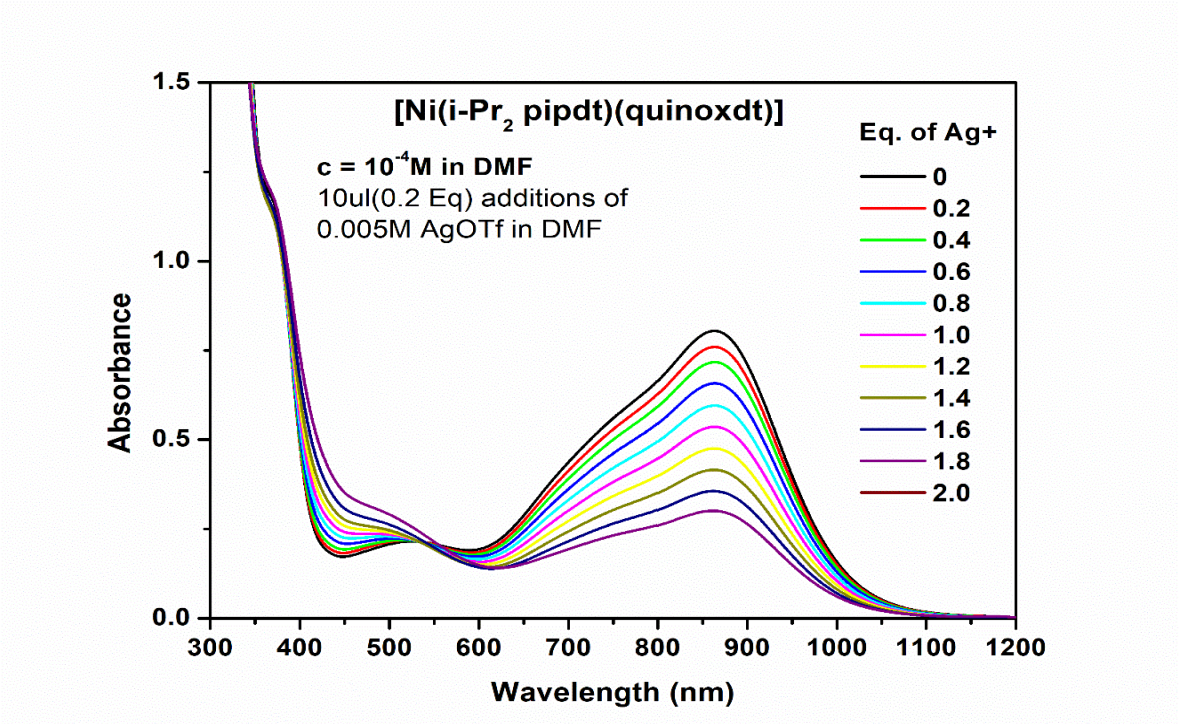

Figure S4. Variation of absorption upon successive additions of silver triflate (10 µL, 5x10^{-3} M) to a solution of **3b** in DMF (2.5mL, 1x10^{-4} M).

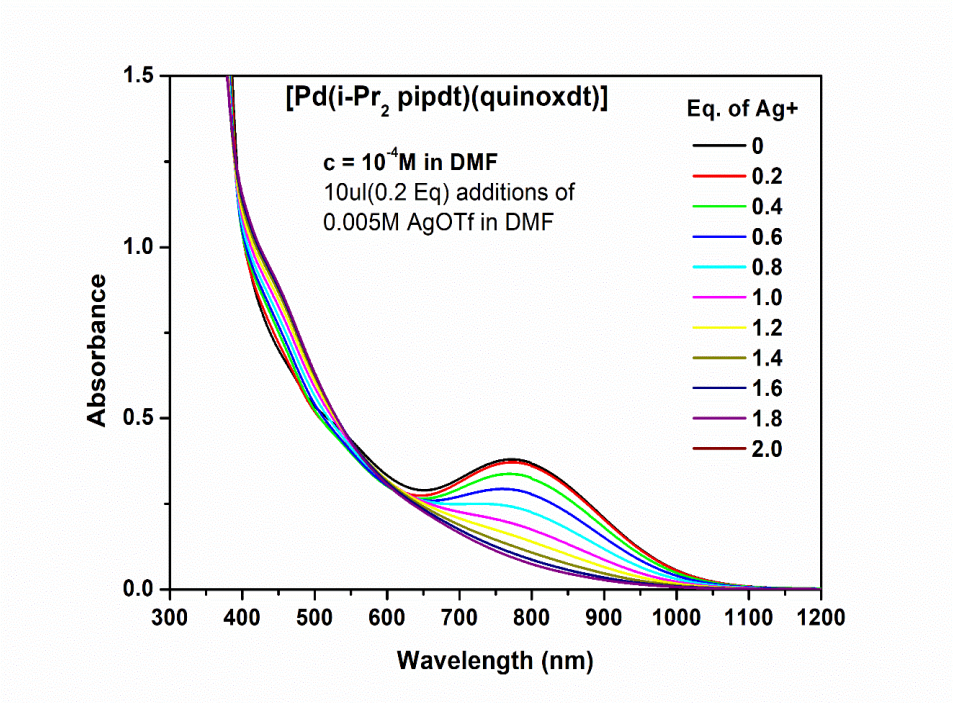

Figure S5. Variation of absorption upon successive additions of silver triflate (10 µL, $5x10^{-3}$ M) to a solution of **3c** in DMF (2.5mL, $1x10^{-4}$ M).

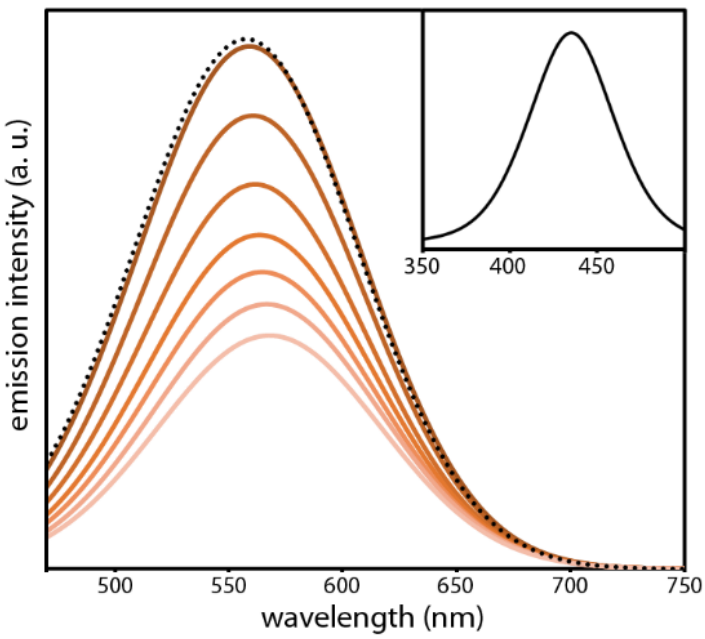

Figure S6 Variation of emission intensity of **3b** in DMF solution (2 mL, $5x10^{-4}$ M) upon successive additions of silver triflate (10 µL, $2x10^{-2}$ M) (blue lines) up to a molar ratio 1.2:1 and of HCl (100 µL, $2.5x10^{-2}$M) (black dotted line). Excitation wavelength was 440 nm. The excitation spectrum acquired by monitoring emission at 570 nm is reported in the inset.

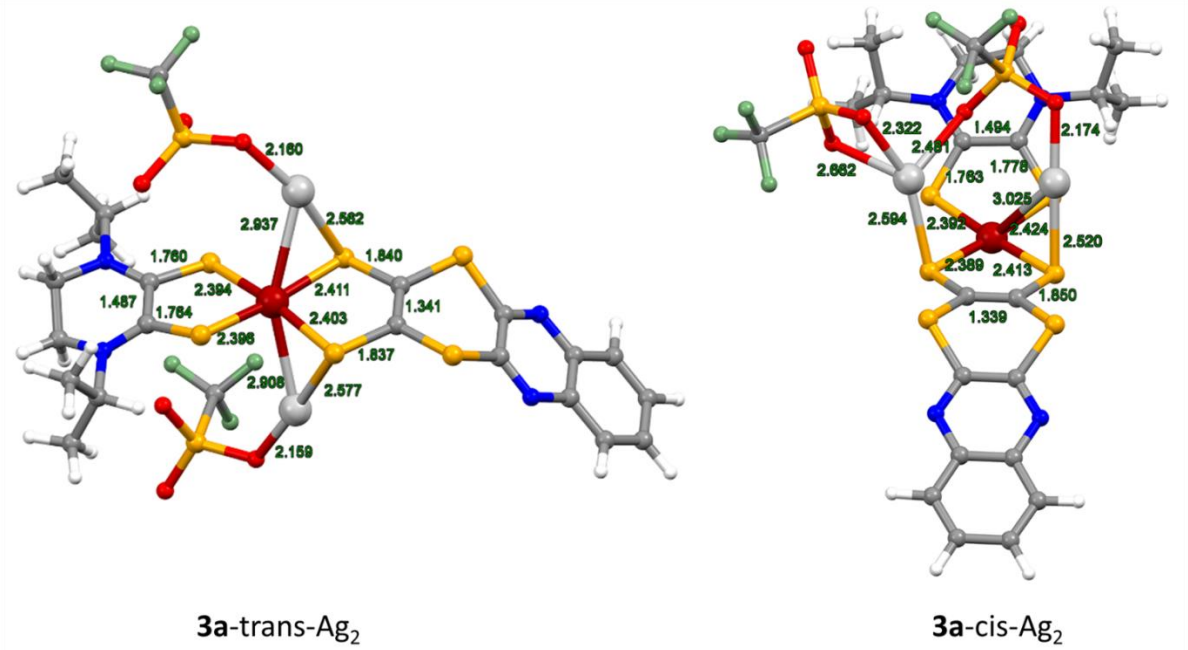

Figure S7. Optimized molecular structures of the two adducts [Pt(i-Pr_2pipdt)(quinoxdt)]·2($AgCF_3SO_3$) in the gas phase (B3LYP/6-31+G(d)-SDD). Selected bond distances are reported in Å.

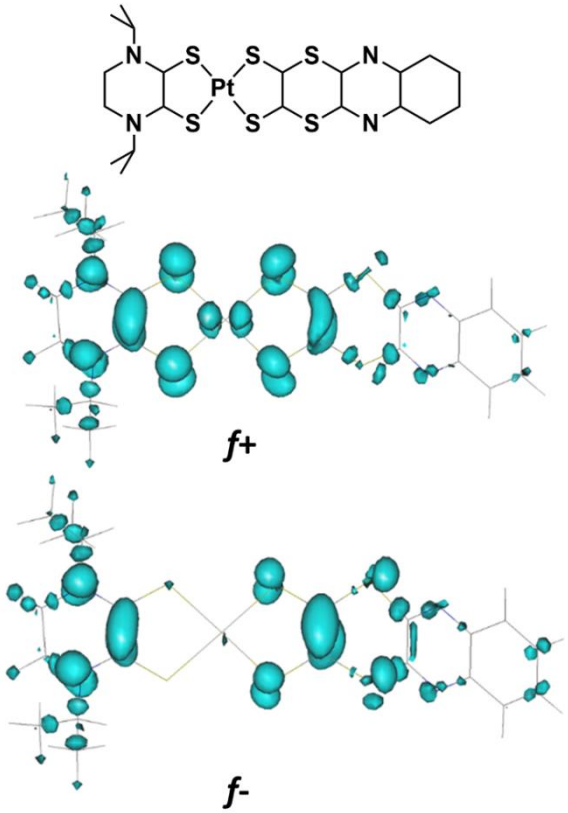

Figure S8. 3D isosurfaces corresponding to the positive and negative Fukui function *f*+ and *f*- for [Pt(i-Pr_2pipdt)(quinoxdt)] (B3LYP/6-31+G(d)-SDD)). The isosurfaces are depicted for a value of + 0.002 e- $Å^{-3}$.

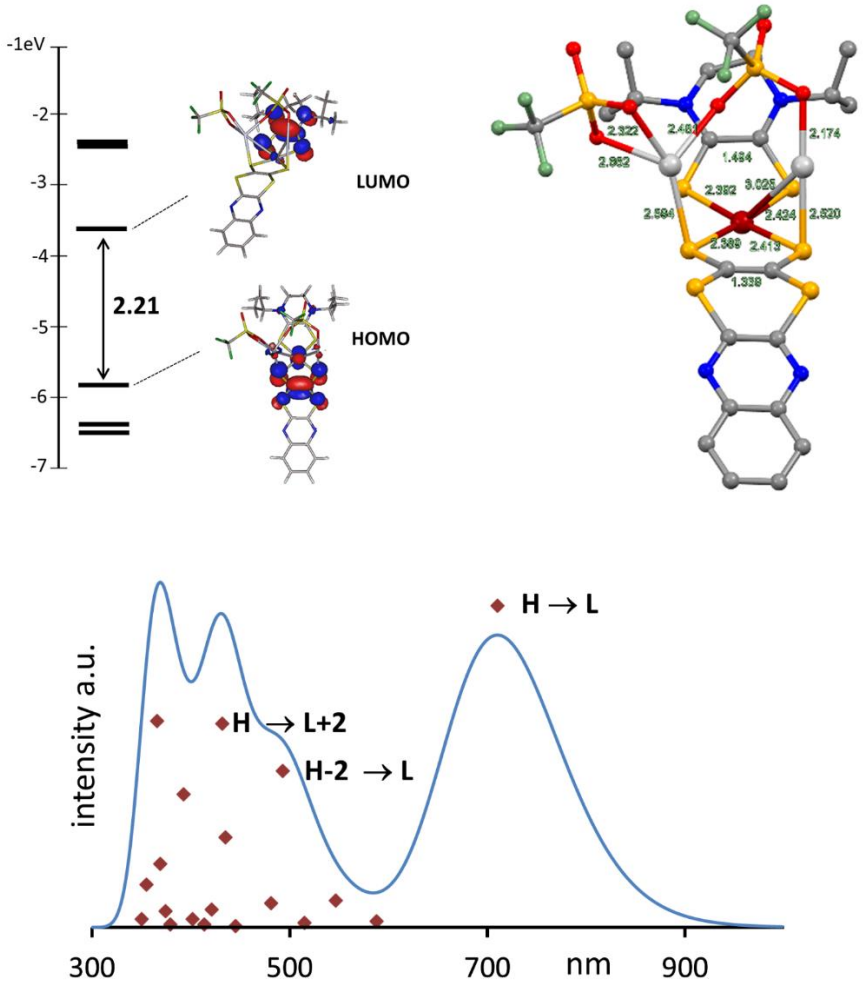

Figure S9. Above, energy levels and shape of the frontier molecular orbitals of the adduct **3a**-cis-Ag_2, together with the optimized geometry. Below, simulated UV-vis spectrum of **3a**-cis-Ag_2 together with the principal singlet transition responsible for the main absorption band in the visible region (red dots). Calculation were performed with the PCM method (DMF), B3LYP/6-31+G(d)-SDD.

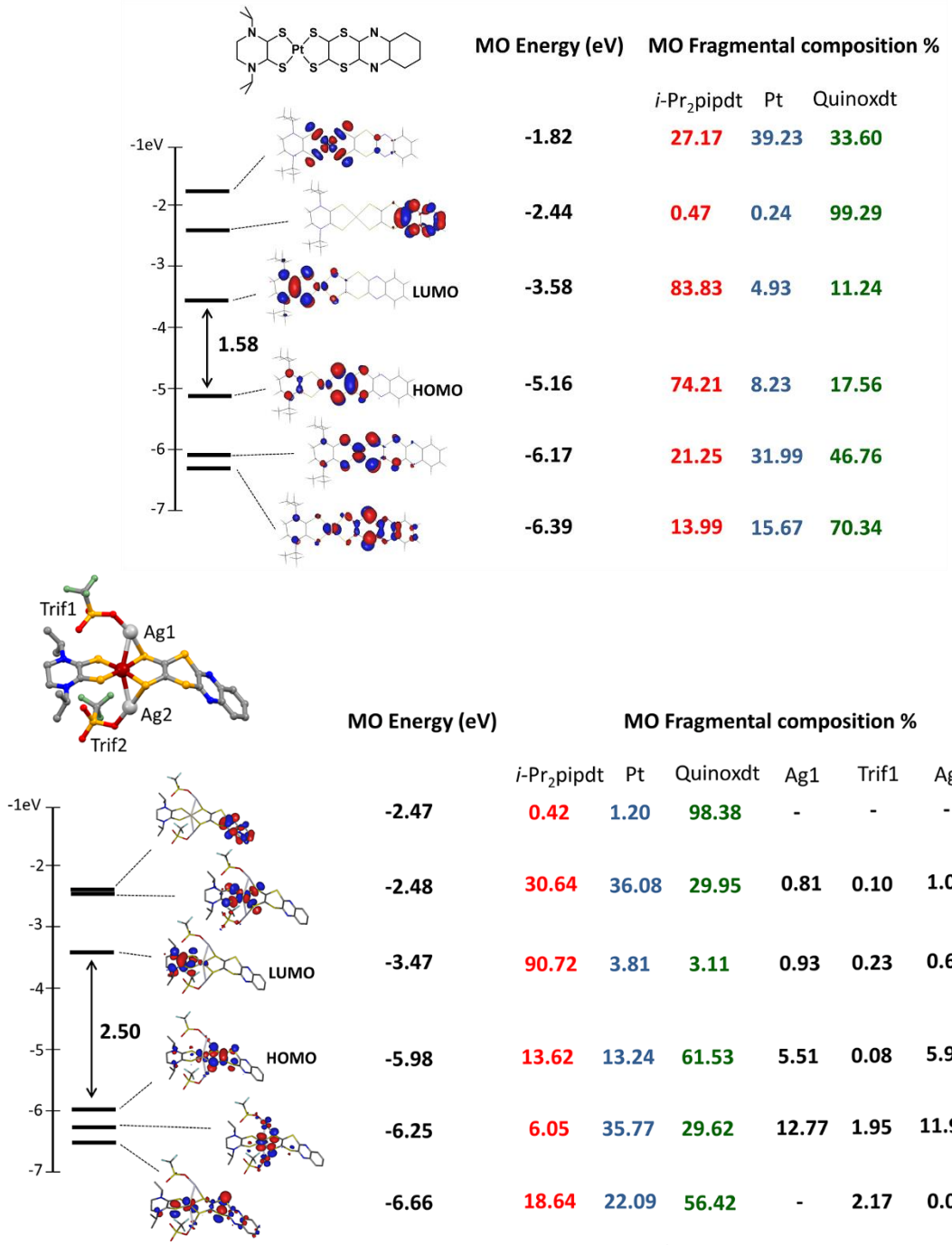

Figure S10. Above, energy (eV) and fragmental composition[1] of the frontier MOs of **3a**. Below, energy (eV) and fragmental composition[1] of the frontier MOs of **3a**-trans-**Ag2.** Computation were performed with the PCM method (DMF), B3LYP/6-31+G(d)-SDD.

[1] S.I.Gorelsky, A.B.P.Lever, J.Organomet.Chem. 635, 187-196 (2001); S.I.Gorelsky, AOMix program, http://www.sg-chem.net/

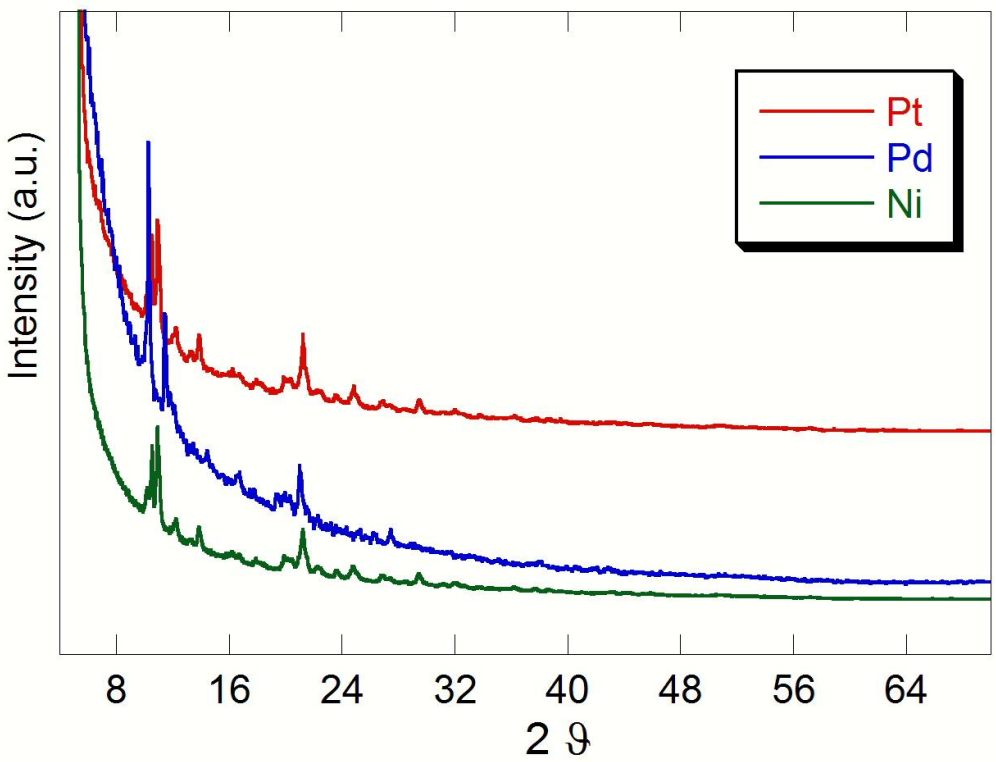

Figure S11. X-ray Powder Diffraction (PXRD) patterns of the Pt-, Pd-, and Ni- complexes. Measurements were performed on a Panalytical Empyrean diffractometer equipped with a graphite monochromator on the diffracted beam and an X'Celerator linear detector. The scans were collected under spinning at 1 Hz within the range of 4°-80° (2θ) using CuKα radiation. PXRD patterns of the Ni- and Pd- complexes show very close resemblance to the PXRD pattern of the Pt- complex, suggesting that isostructural complexes are obtained within the triad (Ni, Pd, Pt).